Journal of Power Sources 191 (2009) 483–488

Contents lists available at ScienceDirect

Journal of Power Sources

journal homepage: www.elsevier.com/locate/jpowsour

Effect of substrate material on the corrosion of TiN-coated stainless steels in simulated anode and cathode environments of proton exchange membrane fuel cells

Yan Wang*, Derek O. Northwood

Department of Mechanical, Automotive, and Materials Engineering, University of Windsor, 401 Sunset Avenue, Windsor, Ontario, Canada N9B 3P4

ARTICLE INFO

Article history:
Received 7 January 2009
Received in revised form 9 February 2009
Accepted 10 February 2009
Available online 20 February 2009

Keywords:
PVD
Bipolar plates
Fuel cells
Corrosion

ABSTRACT

A physical vapor deposition (PVD) TiN coating has been used to increase the corrosion resistance of two stainless steel materials for bipolar plate application in proton exchange membrane fuel cells (PEMFCs). Our earlier studies had shown that a TiN coating on SS410 and SS316L increased the corrosion resistance of SS410 and SS316L significantly. In this study, we examine how the substrate affects the corrosion of TiN-coated stainless steel in the simulated anode and cathode environments. Potentiodynamic and contact resistance test results show that the polarization resistance and contact resistance of TiN-coated SS410 and TiN-coated SS316L are almost the same. However, in the simulated anode condition, the corrosion current density of TiN-coated SS410 is positive and the corrosion current density of TiN-coated SS316L is negative. Inductively coupled plasma optical emission spectrometry (ICP-OES) test results also show that the metal ion concentration is much higher for TiN-coated SS410 at the anode side. At the cathode side, the potentiostatic and ICP-OES tests show that the corrosion of TiN-coated SS410 and TiN-coated SS316L are in the same range. Therefore, the substrate has an effect on corrosion in the simulated anode working conditions of PEMFCs. In order to be the suitable bipolar plate materials, both the coating and substrate need to have a higher corrosion resistance.

1. Introduction

Proton exchange membrane fuel cells (PFMFCs) are regarded as one of the most promising fuel cells for stationary and transportation applications because they operate at low temperatures and allow for rapid start-up [1]. However, their high price prevents PEMFCs from being more widely used. Bipolar plates are one of the most important components in PEMFCs. According to the U.S. Department of Energy (DOE) Annual (2007) review of fuel cells, the cost target in 2015 for bipolar plates is \$3 kW^{-1} out of a total cost of \$30 kW^{-1} for a direct hydrogen fuel cell power system for transportation [2]. Metallic bipolar plates are being widely researched in order to substitute for the non-porous graphite bipolar plates in order to reduce weight, cost and volume [3–18].

Physical vapor deposition (PVD) is one of the most promising coating technologies and is widely used for the improvement of the mechanical and corrosion properties of metallic materials [19]. TiN coatings have been used in many applications, e.g., cutting tools, because of their high wear resistance, hardness and low friction coefficient characteristics [20]. TiN coatings also have potential application to metallic bipolar plates because of TiN's excellent corrosion resistance and metal-like electrical conductivity [21].

In our previous studies [22,23], we have investigated the electrochemical properties of TiN-coated SS410 and TiN-coated SS316L in simulated PEMFC working conditions. The potentiodynamic test results showed that the corrosion resistance of both SS410 and SS316L were increased significantly by coating with TiN. How the substrate affects the physical and electrochemical behaviour of the TiN-coated stainless steel was not addressed in refs. [22,23]. In this study, we report on some experiments designed to the effects of substrate material on the corrosion of TiN-coated stainless steel in simulated anode and cathode environments of PEMFCs.

2. Experimental details

2.1. PVD coating and electrode preparation

SS410 (Martensitic) and SS316L (Austenitic) were chosen as the base materials and the chemical composition of these two stainless steels are shown in Table 1. Austenitic stainless steels normally have better corrosion resistance than ferritic and martensitic stainless steels because the carbides can be retained in solid solution by rapid cooling from high temperature [24]. Comparing the compo-

* Corresponding author. Tel.: +1 519 253 3000x4785; fax: +1 519 973 7007.
E-mail addresses: wang167@uwindsor.ca (Y. Wang), dnorthwo@uwindsor.ca (D.O. Northwood).

0378-7753/$ – see front matter © 2009 Elsevier B.V. All rights reserved.
doi:10.1016/j.jpowsour.2009.02.029

Table 1
Chemical compositions of SS316L and SS410 (wt%).

Metal	C	Mn	P	S	Si	Cr	Ni	Mo	Cu	Co	N	Al	Ti	Sn	Fe
SS316L	0.021	1.82	0.029	0.01	0.58	16.32	10.54	2.12	0.47	–	0.03	–	–	–	Balance
SS410	0.135	0.36	0.018	0.001	0.4	12.22	0.21	0.03	0.1	0.01	0.012	0.001	0.001	0.011	Balance

sition of the two stainless steels, SS316L has a higher content of Ni and Cr. It is well known that the chromium content in a stainless steel determines the corrosion resistance because chromium forms a passive film that can prevent further corrosion. Also, nickel can play an important role in corrosion behaviour of stainless steels. Nickel has a face-centered cubic (FCC) crystal structure and nickel additions allow the stainless steel to retain a FCC structure at room temperature.

SS410 and SS316L were cut into samples of 1.5 cm × 2 cm. Before coating, the metal samples were polished on 240, 320, 400, 600 and 800 grit silicon carbide papers. The coating process was plasma-enhanced reactive evaporation, in which Ti was evaporated in direct current (DC) plasma of nitrogen and argon. The process was conducted at about 450 °C and the total coating time was about 12 h. The samples were drilled a small hole at one edge and suspended over the evaporation from a wire. After PVD coating, the sample was cut into 1.5 cm × 1.5 cm. An electrical contact was made to one side by means of nickel print. Then the contact side and the edges of the metal sample were sealed with epoxy resin, leaving one side for physical and electrochemical characterization [23].

2.2. Characterization of the PVD coatings

The PVD-coated samples were examined by X-ray diffraction (XRD) using a Rigaku X-ray diffractometer operated at V = 30 kV, I = 30 mA and Cu Kα radiation. The surface morphologies were characterized at high magnifications using scanning electron microscopy (SEM) (JEOL JSM-5800LV). The accelerating voltage was 15 kV.

2.3. Electrochemistry of the PVD coatings

In the potentiodynamic tests, the initial potential was −0.1 V vs. open circuit potential (OCP), the final potential was 1.2 V vs. saturated calomel electrode (SCE) and the scan rate was 1 mV s^{-1}. The measurements were carried out at temperature of 70 °C. The polarization resistance was obtained from the polarization curves based on the linear polarization method.

The potentiostatic test applies a constant potential and monitors the current as a function of time. In PEMFCs, the anode and cathode are under different potentials. At the anode, the applied potential was −0.1 V vs. SCE purged with H_2, and at the cathode, the applied potential was 0.6 V vs. SCE purged with O_2. The setting time is 1 or 10 h with 1 point s^{-1} measurement. The temperature for the potentiostatic test was 70 °C.

Electrochemical impedance test uses the Zplot for Windows software package to perform impedance measurements. A ZplotW setup file must already have been created before beginning this experiment. A Solartron Electrochemical Interface (S1 1287) and a frequency response analyzer (FRA) were used to conduct electrochemical impedance spectroscopy (EIS) measurements. The impedance measurements were performed at OCP and the perturbation amplitude was 10 mV. The applied frequencies ranged from 1 M to 10^{-1} Hz, and the data were analyzed by both Zview and ZSmipWin [25] softwares.

2.4. ICP-OES test

Inductively coupled plasma optical emission spectrometry (ICP-OES) (IRIS #701776, Thermo Jarrell Ash Corporation) was used to investigate the metal ion concentrations in the electrolyte solution after corrosion. Liquid samples were introduced into the instrument via a Meinhard concentric glass nebulizer (TK-30-K2, JE Meinhard Associates Inc., California, USA) combined with a cyclonic spray chamber. The aerosol was then introduced into a radial orientation argon plasma resulting in characteristic emission lines that are simultaneously resolved using argon purged echelle optics and a thermostatted charge injection device detector.

2.5. Interfacial contact resistance test

The interfacial contact resistance measurement method that was used in our experiments was based on other researchers' methods [1,26]. All interfacial contact resistance measurements were carried out at room temperature. In our setup, shown in Fig. 1, two pieces of Toray conductive carbon paper (ordered from Fuel Cell Store) were sandwiched between the metal sample and the copper plates. A GW Instel GOM-802 milliohmmeter was used to measure the electrical resistance. While the compaction force was gradually increased, the contact resistance was gradually decreased. The compaction force was applied by means of a Tinus Olsen test machine.

As can be seen in Fig. 1, the total measured resistance (R_{T1}) is a resistance sum including two carbon paper/copper plate interfaces ($R_{C/Cu}$), two carbon paper/metal plate interfaces ($R_{C/M}$), the resistance of the metal (R_M), two carbon paper resistances (R_C) and two copper resistances (R_{Cu}). In order to calculate the contact resis-

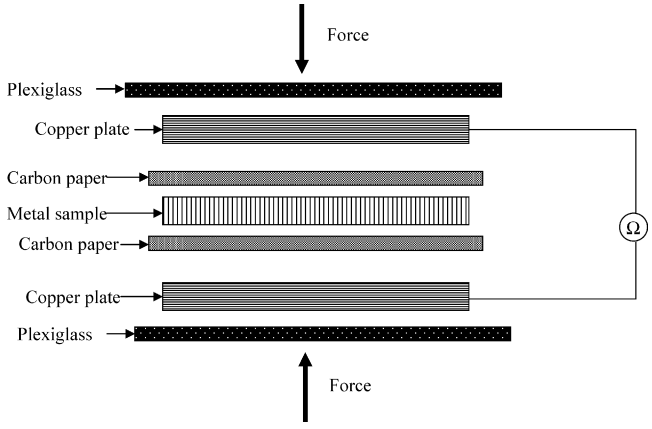

Fig. 1. The setup for resistance 1 measurement.

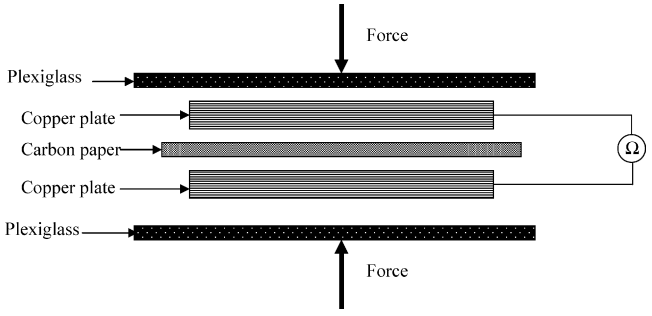

Fig. 2. The setup for resistance 2 measurement.

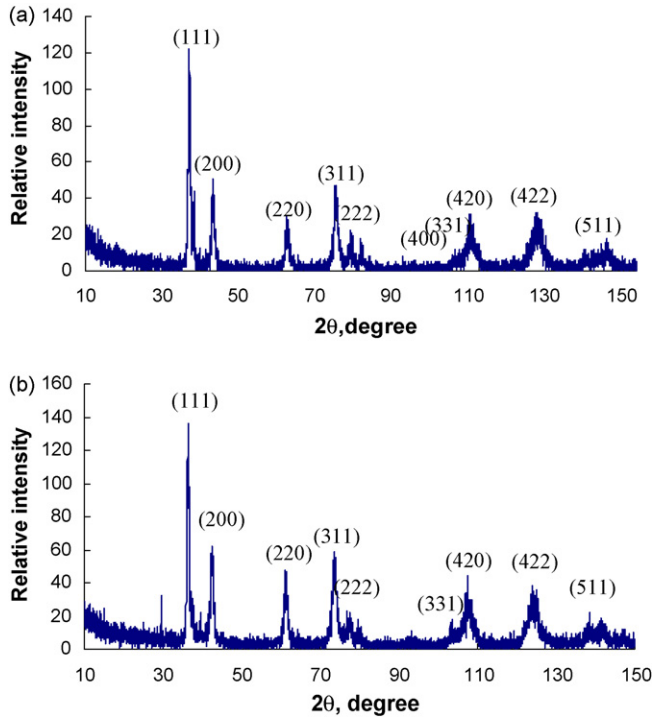

Fig. 3. XRD patterns for TiN-coated SS410 and TiN-coated SS316L, (a) TiN-coated SS410 (b) TiN-coated SS316L.

tance of carbon paper and metal plates, another experiment was set up as in Fig. 2, (the total measured resistance is R_{T2}), which included two carbon paper/copper plate interfaces ($R_{C/Cu}$), one carbon paper/metal plates interface ($R_{C/M}$), the resistance of metal (R_M), one carbon paper resistance (R_C) and part of copper resistance (R_{Cu}).

$$R_{T1} = 2R_{C/Cu} + 2R_{C/M} + R_M + 2R_C + 2R_{Cu} \quad (1)$$

$$R_{T2} = 2R_{C/Cu} + R_C + 2R_{Cu} \quad (2)$$

$$\text{Therefore, } R_{C/M} = \frac{R_{T1} - R_{T2} - R_M - R_C}{2} \quad (3)$$

Since the resistances of the metal and the carbon paper are very small compared to the interfacial contact resistance, Eq. (3) can be rewritten as:

$$R_{C/M} = \frac{R_{T1} - R_{T2}}{2} \quad (4)$$

After this correction, halving the result gives the interfacial contact resistance for the carbon paper/metal ($R_{C/M}$) interface (assuming that the surfaces are homogeneous).

3. Results and discussion

3.1. XRD test

The XRD results for TiN-coated SS410 and TiN-coated SS316L are shown in Fig. 3(a) and (b), respectively. Comparing the two patterns, they have almost the same peaks. The TiN coating has a single-phase structure that is FCC. The XRD peaks from the base materials cannot be seen because the X-rays do not penetrate beyond the TiN coating. From the XRD patterns, the (1 1 1) peak is the strongest; therefore, the growth orientation of TiN is mainly in the (1 1 1) direction.

3.2. SEM test after PVD coating

Fig. 4 presents SEM micrographs of the TiN-coated SS410 and SS316L surface. From the secondary images of the surfaces of TiN-coated on SS410 and SS316L, Fig. 4(a) and (c), we see that TiN has a

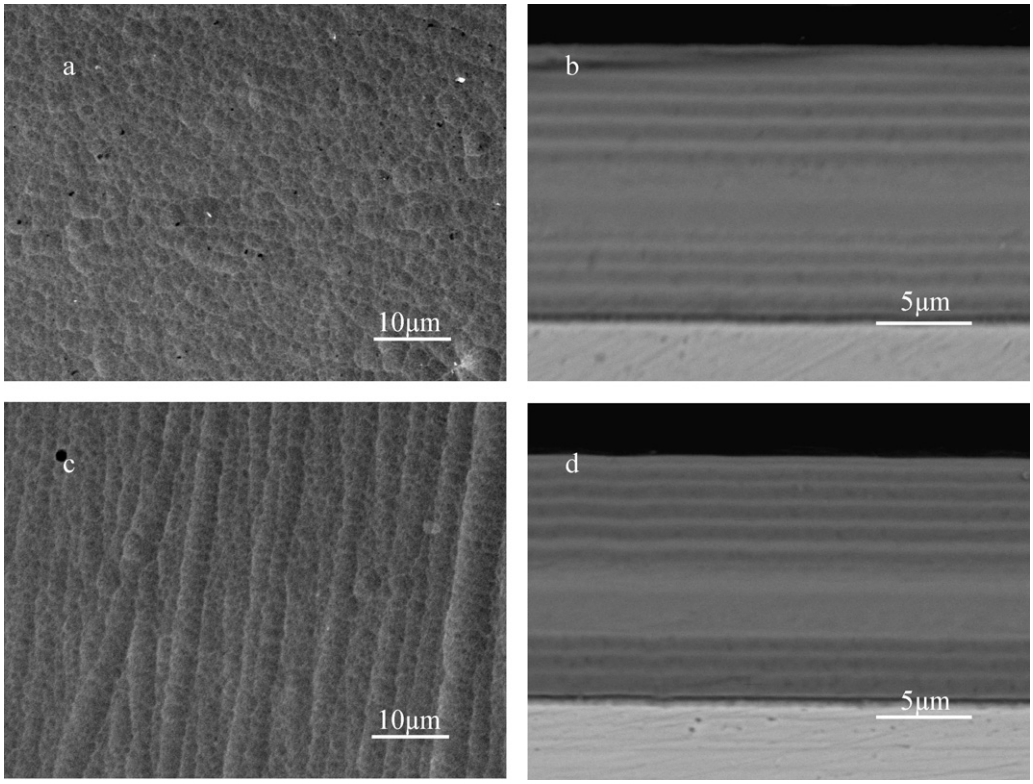

Fig. 4. TiN-coated SS410 and TiN-coated SS316L (a) TiN-coated SS410 surface (secondary electron image), (b) cross-sectional view of TiN coating on SS410 (back scattered electron image), (c) TiN-coated SS316L surface (secondary electron image) and (d) cross-sectional view of TiN coating on SS316L (back scattered electron image).

Table 2
Polarization parameters and protective efficiencies of TiN-coated SS410 and TiN-coated SS316L at 70 °C.

Metal	β_a V^{-1}	β_c V^{-1}	i_{corr}/(μA cm^{-2})	R_p/(Ω cm^2)	Protective efficiency (p_i)
Uncoated SS410	0.199	0.167	188.59	209	N/A
TiN-coated SS410	0.079	0.075	1.750	9559	99.07%
Uncoated SS316L	0.055	0.074	40.318	340	N/A
TiN-coated SS316L	0.224	0.026	1.020	9930	97.47%

dented appearance due to the columnar growth of the TiN during the coating process. Comparing Fig. 4(a) and (c), the morphology of the TiN coating is a little different. If we observe the TiN-coated surfaces carefully, we find that there are pores in the coating (show up as black 'dots'). From the back-scattered electron images of cross-sections of TiN-coated SS410 and SS316L, we see that the TiN coating is multilayered and the coating thickness is about 15 μm, Fig. 4(b) and (d). This layering is because of regular modulation of the N_2 flow and irregular oscillations of the Ti from the e-beam pool during the commercial coating process. These layers overlap and result in a multilayered structure [22,23].

3.3. Potentiodynamic tests

Based on the linear polarization method, we can obtain the polarization parameters for TiN-coated SS410 and TiN-coated SS316L and these are summarized in Table 2. We can see that the polarization resistance, R_p, is almost the same for TiN-coated SS410 and TiN-coated SS316L. However, the polarization current density for TiN-coated SS410 is higher than that of TiN-coated SS316L. Comparing the data in Table 2, we find that the polarization resistance is increased about 30 times after coating TiN for both SS410 and SS316L.

The protective efficiency, P_i, was determined from the polarization curves by

$$P_i(\%) = 100\left(\frac{1 - i_{cor}}{i^0_{cor}}\right) \quad (5)$$

Where i_{cor} and i^0_{cor} denote the corrosion densities in the presence and absence of the coating, respectively [27,28]. The protective efficiency results are also shown in Table 2. From Table 2, we can see that the protective efficiency of the TiN coating on SS410 is slightly higher than on SS316L, primarily because the polarization current density of uncoated SS410 is higher.

3.4. Potentiostatic tests

Fig. 5(a) presents the potentiostatic test results in the simulated anode conditions. For TiN-coated SS316L, the corrosion current density is negative. For TiN-coated SS410, the corrosion current density is negative at the beginning, but after 20 s, the corrosion current density of TiN-coated SS410 becomes positive. As we have discussed in our earlier papers [22,23,29,30,31], the negative current can provide cathodic protection for the substrate and the positive current is because of the metal corrosion. Corrosion takes place because the sulphuric acid penetrates to the substrate through the micro-pores and pinholes existing in the TiN coatings [32,33,34]. From Fig. 5(b), which is the cathode side, we can see that the corrosion current density is positive for both TiN-coated SS410 and TiN-coated SS316L. Also, the corrosion current density is higher for TiN-coated SS410 than for TiN-coated SS316L for times up to 2500 s. After 2500 s, the TiN-coated SS410 and TiN-coated SS316L have almost the same corrosion current density.

3.5. SEM examination after 10 h potentiostatic tests in simulated anode and cathode conditions

Fig. 6 presents the SEM images of TiN-coated SS410 and TiN-coated SS316L after 10 h potentiostatic tests in the simulated anode and cathode conditions. There are no apparent corrosion products on these SEM images because the corrosion current density is very low, but the surface morphology changes after the potentiostatic tests. Comparing Fig. 6(a) and (b), we can still see the dented structure after 10 h potentiostatic testing in the simulated cathode environments. This means that corrosion is more severe in the anode side for TiN-coated SS410. Comparing Fig. 6(c) and (d), we see that there is a greater change in surface appearance after 10 h potentiostatic testing in the simulated cathode environment than the anode. Thus, corrosion is more severe in the cathode side for TiN-coated SS316L. This will be discussed further in Section 3.7.

3.6. EIS test

Fig. 7 presents the electrochemical impedance spectra for TiN-coated SS410 and TiN-coated SS316L. Comparing the two curves in Fig. 7(a), we can see that the real component of the electrochemical impedance spectra for TiN-coated SS410 is higher. However, the imaginary component of the electrochemical impedance spectra for TiN-coated SS316L is higher. The resistance part is higher for TiN-coated SS316L and capacitance part is higher for SS410. From Fig. 7(b), we can see that in the low frequency range, the total resistance of TiN-coated SS316L is slightly higher. In the high frequency,

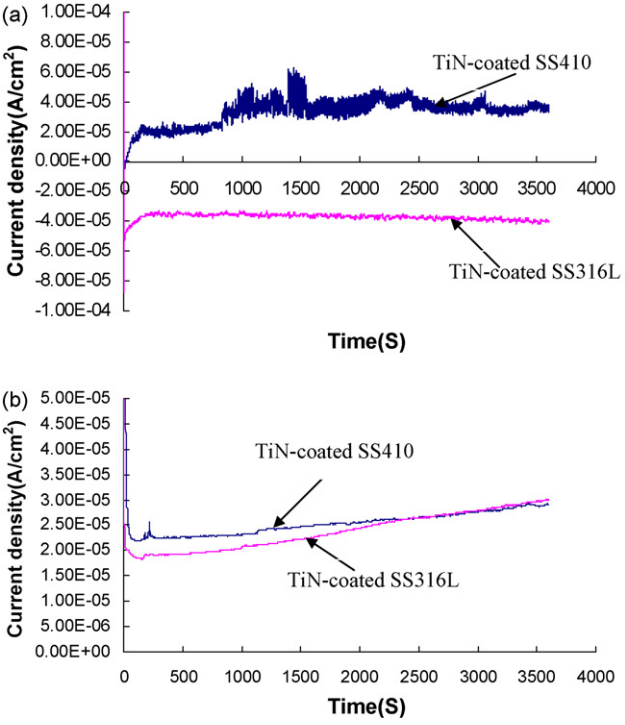

Fig. 5. Potentiostatic tests for TiN-coated SS410 and TiN-coated SS316L at 70 °C in a 0.5 M sulphuric acid solution, (a) anode side and (b) cathode side.

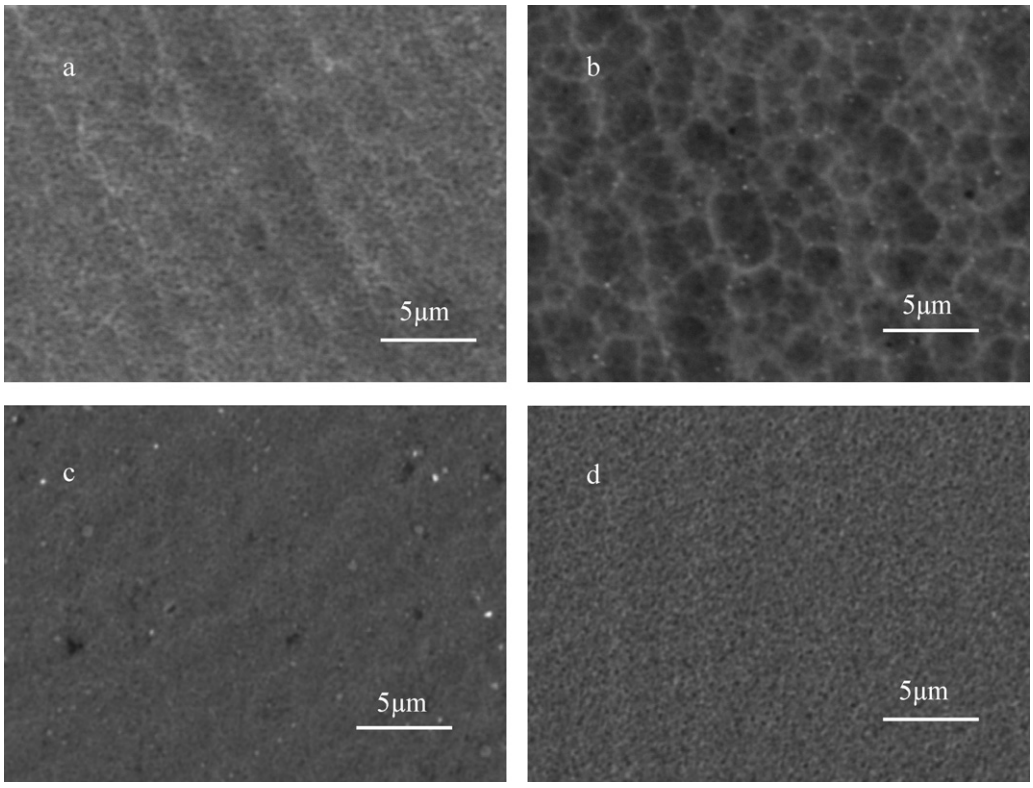

Fig. 6. SEM micrographs for TiN-coated SS410 and TiN-coated SS316L after 10 h potentiostatic tests in the simulated anode and cathode environments; (a) TiN-coated SS410 at anode side, (b) TiN-coated SS410 at cathode side, (c) TiN-coated SS316L at anode side and (d) TiN-coated SS316L at cathode side.

the two curves merge together. Therefore, TiN-coated SS316L has a higher electrochemical impedance.

3.7. ICP-OES test

Table 3 presents the metal ion concentrations after 10 h potentiostatic testing in the simulated anode and cathode environments. Base solution is distilled water. We can see that the metal ion concentration in the simulated cathode condition is higher for TiN-coated SS316L. However, for TiN-coated SS410, the metal ion concentration in the simulated anode condition is much higher. Also, we can see that the metal ion concentration of TiN-coated SS410 at anode side is very high. However, the metal ion concentration of TiN-coated SS316L at anode side is low because the negative current can provide partial protection for the samples.

The other important observation is the presence of Ti ions, which can account for up to 19.5% of the total metal ion concentration. These Ti ions would have originated from the dissolution of the TiN PVD coating. A less corrosion resistant substrate, SS410, also gave rise to a higher Ti ion concentration. The Ti ion concentration values are consistent with the SEM observations at the surface, Fig. 6. For TiN-coated SS410, there was a greater change in the surface appearance at the anode, Fig. 6a, than at the cathode, Fig. 6b. The reverse was true for TiN-coated SS316L, where a greater change in surface appearance was seen at the cathode, Fig. 6d, together with a higher Ti ion concentration.

3.8. Interfacial contact resistance test

Table 4 summarizes the interfacial contact resistance results for TiN-coated SS410 and TiN-coated SS316L. With increasing compaction pressure from 22 N cm^{-2} to 222 N cm^{-2}, the contact resistance decreased rapidly at low compaction pressures and then decreased more gradually, probably due to a decrease in interfacial resistance [35]. Comparing the data in Table 4, we can see that the contact resistance is almost the same for TiN-coated SS410 and TiN-coated SS316L. After TiN coating, the contact resistance is higher than desired. A possible reason for this is that the TiN coatings have a multilayered structure and the interfaces between could increase the contact resistance.

Table 3
Metal ion concentration of TiN-coated SS410 and TiN-coated SS316L after 10 h potentiostatic tests in the simulated anode and cathode environments.

Different coatings	Dissolved metal concentration (μg L^{-1})					Total concentration of metal ions (μg L^{-1})
	Fe	Ti	Cr	Ni	Mn	
Base solution	20.71	<IDL	<IDL	<IDL	1.36	22.07
TiN-coated SS410 at anode side	38410 (69.5%)[a]	10320 (18.7%)	4990 (9.0%)	570 (1.0%)	1000 (1.8%)	55290
TiN-coated SS410 at cathode side	2660 (72.1%)	720 (19.5%)	240 (6.5%)	60 (1.6%)	10 (0.3%)	3690
TiN-coated SS316L at anode side	370 (71.8%)	25 (4.9%)	50 (9.7%)	60 (11.7%)	10 (1.9%)	515
TiN-coated SS316L at cathode side	1900 (68.3%)	410 (14.7%)	290 (10.4%)	70 (2.5%)	110 (4.0%)	2780

IDL, identification limit.
[a] ()% of total metal ion concentration.

Table 4
Interfacial contact resistance for TiN-coated SS410 and TiN-coated SS316L.

Compaction force ($N\,cm^{-2}$)	22	44	67	89	111	133	156	178	200	222
Contact resistance for TiN-coated SS316L ($m\Omega\,cm^2$)	884	359	161	138	119	106	100	99	88	78
Contact resistance for TiN-coated SS410 ($m\Omega\,cm^2$)	887	361	162	139	118	106	100	98	87	78

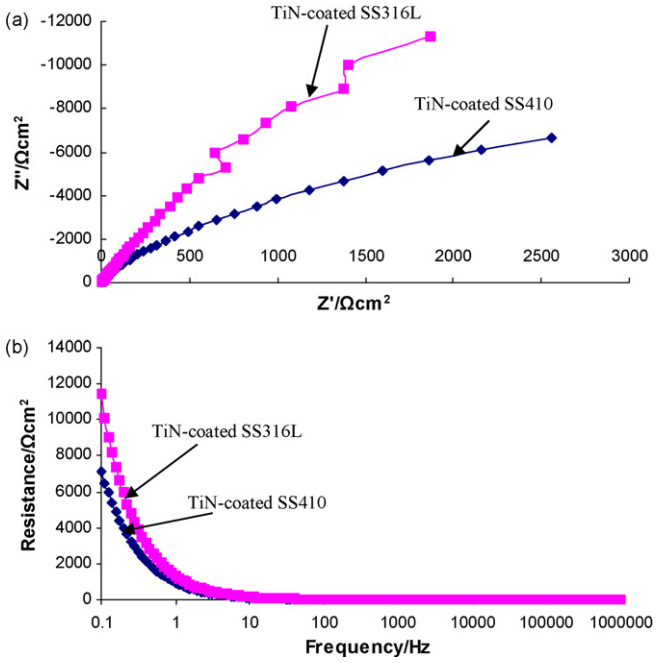

Fig. 7. Electrochemical impedance spectra for TiN-coated SS410 and TiN-coated SS316L (a) Nyquist plot and (b) Bode plot.

4. Conclusions

The physical and electrochemical characteristics of TiN-coated SS410 and TiN-coated SS316L were compared in this study. Both materials have similar XRD patterns, coating thicknesses, polarization resistance and interfacial contact resistance. However, the corrosion current density of TiN-coated SS410 and TiN-coated SS316L is quite different. In the simulated anode side, the corrosion current density of TiN-coated SS410 is positive due to the corrosion. The corrosion current density of TiN-coated SS316L is negative, which can provide partial protection for the substrate. ICP-OES measurements of metal ion concentrations show a significant fraction of Ti ions (up to 19.5%). These Ti ions would arise from dissolution of the TiN coating. A less corrosion-resistant substrate, SS410, led to higher Ti ion concentrations. Therefore, the substrate does have effects on the corrosion behaviour for TiN-coated stainless steel. In order to be suitable bipolar plate materials, not only should the coating have very high corrosion resistance, but also the substrate should have excellent corrosion resistance.

Acknowledgements

The research was financially supported by the Natural Sciences and Engineering Research Council of Canada (NSERC) through a Discovery Grant awarded to Professor D.O. Northwood. Yan Wang would like to acknowledge financial support through an Ontario Graduate Scholarship.

References

[1] D.P. Davies, P.L. Adcock, M. Turpin, S.J. Rowen, J. Appl. Electrochem. 30 (2000) 101–105.
[2] http://www1.eere.energy.gov/hydrogenandfuelcells/mypp/pdfs/fuel_cells.pdf. Last retrieved on February 8, 2009.
[3] H. Wang, J.A. Turner, J. Power Sources 128 (2004) 193–200.
[4] H. Wang, G. Teeter, J. Turner, J. Electrochem. Soc. 152 (3) (2005) B99–B104.
[5] A.M. Lafront, E. Ghali, A.T. Morales, Electrochim. Acta 52 (2007) 5076–5085.
[6] V.V. Nikam, R.G. Reddy, J. Power Sources 152 (2005) 146–155.
[7] V.V. Nikam, R.G. Reddy, Electrochim. Acta 51 (2006) 6338–6345.
[8] J. Wind, R. Späh, W. Kaiser, G. Böhm, J. Power Sources 105 (2002) 256–260.
[9] E.A. Cho, U.-S. Jeon, S.-A. Hong, I.-H. Oh, S.-G. Kang, J. Power Sources 142 (2005) 177–183.
[10] S. Lee, C. Huang, J. Lai, Y. Chen, J. Power Sources 131 (2004) 162–168.
[11] N. Cunningham, D. Guay, J.P. Dodelet, Y. Meng, A.R. Hlil, A.S. Hay, J. Electrochem. Soc. 149 (7) (2002) A905–A911.
[12] H. Wang, M.P. Brady, G. Teeter, J.A. Turner, J. Power Sources 138 (2004) 86–93.
[13] H. Wang, M.P. Brady, K.L. More, H.M. MeyerIII, J.A. Turner, J. Power Sources 138 (2004) 79–85.
[14] D.R. Hodgson, B. May, P.L. Adcock, D.P. Davies, J. Power Sources 96 (2001) 233–235.
[15] P.L. Hentall, J.B. Lakeman, G.O. Mested, P.L. Adock, J.M. Moore, New materials for polymer electrolyte membrane fuel cell current collectors, J. Power Sources 80 (1999) 235–241.
[16] K.M. El-Khatib, M.O.A. Helal, A.A. El-Moneim, H. Tawfik, Anti-Corros. Methods Mater. 51 (2004) 136–142.
[17] S. Lee, C. Huang, Y. Chen, J. Mater. Process. Technol. 140 (2003) 688–693.
[18] M.P. Brady, K. Weisbrod, I. Paulauskas, R.A. Buchanan, K.L. More, H. Wang, M. Wilson, F. Garzon, L.R. Walker, Scripta Mater. 50 (2004) 1017–1022.
[19] L.A. Dobrzański, K. Lukaszkowicz, A. Zarychta, L. Cunha, J. Mater. Process. Technol. 164–165 (2005) 816–821.
[20] Y. Li, L. Qu, F. Wang, Corros. Sci. 45 (2003) 1367–1381.
[21] M. Li, S. Luo, C. Zeng, J. Shen, H. Lin, C. Cao, Corros. Sci. 46 (2004) 1369–1380.
[22] Y. Wang, D.O. Northwood, J. Power Sources 165 (2007) 293–298.
[23] Y. Wang, D.O. Northwood, Int. J. Hydrogen Energy 32 (2007) 895–902.
[24] W.F. Smith, Foundations of Materials Science and Engineering, Third ed., McGraw-Hill, New York, 2004, pp. 497.
[25] http://www.echemsw.com/. Last retrieved on July 30, 2008.
[26] H. Wang, M.A. Sweikart, J. Power Sources 115 (2003) 243–251.
[27] K. Aramaki, Corros. Sci. 41 (1999) 1715–1730.
[28] K. Nozawa, K. Aramaki, Corros. Sci. 41 (1999) 57–73.
[29] Y. Wang, D.O. Northwood, Electrochim. Acta 52 (2007) 6793–6798.
[30] Y. Wang, D.O. Northwood, J. Power Sources 163 (2006) 500–508.
[31] Y. Wang, D.O. Northwood, J. Power Sources 175 (2008) 40–48.
[32] C. Hsu, M. Chen, K. Lai, Mater. Sci. Eng. A 421 (2006) 182–190.
[33] D.A. Jones, Principles and Prevention of Corrosion, First ed., Macmillan, New York, 1992, pp. 147.
[34] F. Lang, Z. Yu, Surf. Coat. Technol. 145 (2001) 80–87.
[35] E.A. Cho, U.S. Jeon, S.A. Hong, I.H. Oh, S.G. Kang, J. Power Sources 142 (2005) 177–183.